IEEE Access
Multidisciplinary ⋮ Rapid Review ⋮ Open Access Journal

Received 12 December 2022, accepted 13 January 2023, date of publication 23 January 2023, date of current version 30 January 2023.

Digital Object Identifier 10.1109/ACCESS.2023.3239303

RESEARCH ARTICLE

Optimal Sizing and Siting of PV and Battery Based Space Microgrids Near the Moon's Shackleton Crater

DIPTISH SAHA[1], (Student Member, IEEE), NAJMEH BAZMOHAMMADI[1], (Member, IEEE), JOSÉ MAURILIO RAYA-ARMENTA[1], ANGELINA D. BINTOUDI[2], (Member, IEEE), ABDEREZAK LASHAB[1], (Senior Member, IEEE), JUAN C. VASQUEZ[1], (Senior Member, IEEE), AND JOSEP M. GUERRERO[1], (Fellow, IEEE)

[1]Center for Research on Microgrids (CROM), AAU Energy, Aalborg University, 9220 Aalborg, Denmark
[2]School of Electrical and Computer Engineering, Aristotle University of Thessaloniki, 54124 Thessaloniki, Greece

Corresponding author: Diptish Saha (dsa@energy.aau.dk)

This work was supported by VILLUM FONDEN through the VILLUM Investigator Grant, Center for Research on Microgrids (CROM), under Grant 25920.

ABSTRACT Space mission cost and feasibility depend mainly on the size and mass of the payload. This paper investigates the optimal photovoltaic (PV) array and battery size and mass for an islanded PV-battery powered space microgrid (MG) at the lunar south pole. The PV arrays are considered to be installed on top of towers to increase solar energy harvesting. Considering the dependency of the generated power from PV arrays on the tower height, different tower heights of 10, 50, and 100 m are investigated. The paper presents the methodology to estimate the available power from the PV system using the information of illumination time-series at the location of potential sites with different tower heights. Besides, considering the power demand of several power-consuming units at different operating states, the power demand profile of the lunar base is generated. The optimal sizing of the PV and battery system for a 1-year horizon, without considering battery degradation, results in a total mass of approximately 1.5×10^5 kg to 3.5×10^5 kg with a tower height of 10 m depending on the solar illumination profiles at different sites. For a 5-year optimization horizon of the same sites with 10 m tower height and considering the battery yearly capacity degradation, total system mass ranges approximately from 2×10^5 kg to 5.5×10^5 kg. Although increasing the tower height may considerably reduce the total size and mass of the battery and PV system, the mass of the PV tower will increase. Thus, a satisfactory trade-off in selecting the site location and tower height is required. In this regard, 15 highly illuminated sites at different locations and with different PV tower heights are assessed in this paper. To improve the reliability and flexibility of the power system, the multi-microgrid (MMG) concept is deployed to distribute the power-consuming units of the base among different MGs having their local energy production and storage systems. Finally, based on the total power demand served at a candidate site and the corresponding total system mass, a criterion, mass-per-unit-load (MPUL), is used to identify the sites that serve the highest power demand with less total system mass.

INDEX TERMS Space microgrids, lunar microgrids, power system sizing, site selection, lunar power system, lunar base, Shackleton crater.

I. INTRODUCTION

Several space agencies such as National Aeronautics and Space Administration (NASA), Japan Aerospace Exploration Agency (JAXA), and China National Space Administration (CNSA) are planning to organize space missions to establish human habitats on the Moon starting from 2024 [1], 2030 [2], [3], and 2036 [4], respectively. Several other space organizations also have similar interests in setting up human bases [5], [6] or heavy industries [7] on the Moon.

The associate editor coordinating the review of this manuscript and approving it for publication was Md. Rabiul Islam.

This growing interest demands the development of electrical power systems on the Moon.

A lunar base includes different power-consuming units such as habitat, life support system (LSS), laboratories, in-situ resource utilisation (ISRU) to utilize lunar resources for an extended stay, as well as electrical rovers and vehicles [8], [9], [10]. Thereby, efficient energy resources are needed to provide the lunar base with the required power. Energy storage systems (ESSs) are also necessary to supply the loads during eclipses and nighttimes. Considering the hostile environment of space, designing a reliable and efficient power system and coordinating several energy resources and electrical equipment in such a complex system with various requirements are very challenging tasks. Also, it might not always be possible to involve crew members having expertise in all areas [11]. Therefore, an autonomous power system ensuring reliability, resiliency, robustness, optimality, and stability (RRROS) is highly required [12]. A lunar electrical power system consisting of interconnected loads, energy generation resources, and ESS can be called a **space microgrid (MG) on the Moon** [8]. Moreover, different power-consuming units in a space MG can be distributed into several MGs having their local power generation and storage system to form an multi-microgrid (MMG) system. The resources in an MMG system can be shared among the MGs to increase the flexibility and reliability of the power system. Given the similarities of terrestrial MGs and space MGs on the Moon, the design and operation management strategies developed for terrestrial MGs can also be implemented in space MGs and vice versa, when possible [13].

On the Moon, due to the scarcity of resources, electric power can be generated from a few sources such as solar radiation, nuclear resources [9], and electrostatic charge from lunar regolith [14]. Nuclear fission-based kilopower reactors are modular, light in mass, small in size and volume, and independent of the site location and illumination conditions. Nevertheless, nuclear kilopower reactors need specific shielding and must be installed at an appropriate distance from the base to reduce the crew's exposure to nuclear radiation [9]. Moreover, disposing of nuclear waste creates additional challenges and environmental issues. Generating power from lunar regolith electrostatic charge is still under laboratory tests [14]. On the other hand, Moon's atmosphere-less environment allows abundant solar energy to reach the lunar surface, where the solar radiations are not affected by environmental factors such as cloud coverage and atmospheric diffusion. Moreover, solar photovoltaic (PV) systems do not require additional heavy infrastructure for shielding, can be easily expanded, and are well tried and tested in space. Although several spacecraft and rovers use nuclear radioisotope thermo-electric generator systems for power generation [15], [16], the only habitable environment in space International Space Station (ISS) still uses solar PV arrays along with rechargeable batteries [17]. Installing solar power facilities for lunar bases is investigated in [18] and [19].

There are several potential locations on the Moon to establish a lunar base which are studied in the literature considering the solar illumination of the sites. The authors of [20] discuss the optimum size of the ESS depending on the average solar illumination of candidate sites and the worst and best case lunar days using Earth-based radar digital elevation model (DEM). In [21], the possibility of installing solar panels on top of towers is studied to increase the average available illumination at a particular location, thereby reducing the ESS requirements. Batteries and regenerative fuel cells (RFCs)-assisted solar arrays are compared in [22] for a 10-year period from 2020 and 2030. It is observed that although the RFC-assisted solar array system has less overall system mass, RFCs has a lower efficiency than batteries. Higher efficiency of batteries results in recharging them faster during short illumination periods. All of these studies rely mainly on the average illumination at these sites and investigate the possibility of reducing the ESS size at highly illuminated lunar locations. Power system design along with sizing of power generation and storage units for a manned-lunar base, are discussed in [13]. In [9], considering one lunar month ($\sim$708 hours), it is shown that the battery mass for a PV-battery power system is approximately 58, 000 kg. A comparison with a PV-RFC power system is also presented. In [9], a lunar site located at 30° latitude with 25.8 kW constant power demand is considered. However, according to previous studies, high latitude ($\sim 85° - 90°$) lunar polar sites are highly illuminated and, thereby, good potential candidates for establishing a lunar base. Moreover, non-polar lunar locations experience approximately 15 days with continuous solar availability followed by approximately 15 days of continuous nighttime [10]. Thereby, the need for large ESSs increases as the power demand by the critical loads during the nighttime should be supplied from the ESSs. Also, the optimization horizon of one lunar month ($\sim$ 708 *hours*) considered in [9] is rather small for sizing an electrical power system.

Different locations on the Moon have different solar power availability depending on the surrounding terrain and solar elevation angle. Several studies [23], [24], [25] have reported average illumination of some highly illuminated locations near the lunar polar regions over a certain period of time. To the best of our knowledge, sizing of a PV-battery-based lunar power system for an extended stay of $\sim$ 1 *year* or more at these locations is not reported in the literature. Besides, although the average illumination gives an approximation of the solar availability, the high terrain and low solar elevation angle near the lunar polar regions create long shadows [21], [26] and obstruct the solar energy availability. Therefore, a more accurate analysis for designing the power system of a lunar base can be achieved by considering the solar illumination time-series profile at the candidate location. Thus, extending the work by the authors of [9], this paper investigates the solar power availability at 15 highly illuminated locations on the lunar polar regions using solar illumination time-series profiles. The information on the

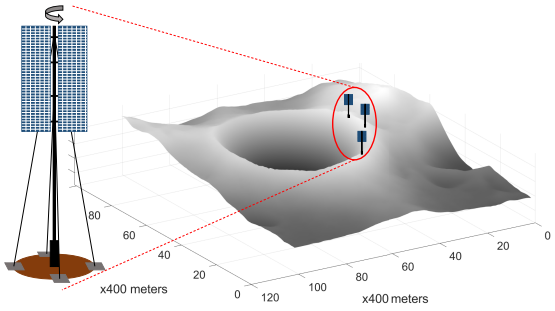

FIGURE 1. Installing solar panels on towers on the rim of craters.

power demand profile is crucial in sizing a power system to maintain the power balance. In [9], the authors consider a constant power demand of a certain power-consuming unit during the lunar daytime and nighttime. However, a power demand profile considering the operation of several power-consuming units in a lunar base is more practical. Therefore, this paper proposes a methodology to generate the power demand profile considering different power-consuming units in the lunar base and the candidate location's daytime and nighttime. As space mission costs are highly dependent on the mass of payload, this paper further proposes an optimization problem to minimize the PV-battery system's mass along with the total cost per day of the battery, considering the illumination time-series and power demand profile at the corresponding lunar location. This paper also considers the yearly battery capacity fading due to the calendar and cyclic aging for an optimization horizon of 5 years. The optimization problem is modeled and solved using *Matlab-fmincon* optimization tool. Moreover, different candidate locations are compared in terms of the required battery size and mass, PV size and mass, average illumination, longest continuous night, total PV power generation, and the total power demand served. It is observed that both PV array area (in m^2) and mass (in kg) are in the order of 10^2, battery size (in Wh) is in the order of 10^7, and both the battery and total PV-battery system mass (in kg) are in the order of 10^5. Therefore, the main contribution of the paper is to propose an optimization framework to optimally size a PV-battery-based electrical power system at a candidate location considering the PV array and battery mass along with the total cost per day of the battery, illumination time-series and power demand profile for 1 year and 5 years optimization horizons. The paper also investigates the possibility of distributing the power-consuming units of a lunar base into several MGs and establishing an MMG system to increase the flexibility, efficiency, and reliability of the system. Finally, the paper proposes a metric mass-per-unit-load (MPUL) based on the total system mass and total power demand served at a location to identify the best site serving the highest power demand with the least total system mass.

The rest of this paper is organized as follows. Assessing solar illumination profiles at different locations on the Moon is presented in Section II where 15 highly illuminated sites at the lunar south pole are considered. In Section III, the methodology for estimating the PV power generation on the Moon, is discussed. Different power consumption units of a lunar base, distributing them into several MGs, and the process of creating the power demand profile are presented in Section IV. Section V is dedicated to the battery and PV sizing and optimization process, along with presenting battery capacity degradation. The comparative analysis of the candidate sites is provided in Section VI. Finally, concluding remarks are given in Section VII.

II. SOLAR ILLUMINATION ON THE MOON

Solar illumination on the Moon depends on different factors such as site topography, solar irradiance profile, and partial and total eclipses. Sites with long illumination and short darkness periods are preferred to reduce the mass and size of the ESS, thereby lowering the lunar base's establishment cost. Different space missions such as *Lunar Reconnaissance Orbiter (LRO)* and *Clementine* by NASA and *Kaguya* by JAXA have helped identify several highly illuminated locations on the rim of the "*Peary*" [9] and "*Shackleton*" [13] craters near the lunar North and South poles, respectively. Some of the sites near the *Shackleton crater* are identified to have a continuous illumination of about six months and frequent illumination-darkness periods for another six months [22] with continuous eclipse times varying from 71 to 120 hours [21], [22]. In the non-polar regions, solar illumination is available continuously for 15 days, followed by 15 days of continuous nighttime (earth days) [10]. Therefore, polar areas are preferred more to establish a lunar base.

Due to the lack of atmosphere on the Moon, meteorites threaten the safety of the lunar base. From the limited data collected by spacecraft and radars, it is identified that the probability of meteoroid fluxes at non-polar lunar latitudes (0°–30°) are higher by 10% compared to polar latitudes (60°–90°) [27]. Although polar regions have a lower probability of getting stricken by meteorites, its possibility cannot be overlooked, and therefore appropriate shielding strategies are needed [28], [29]. Thus, polar regions have the advantages of higher illumination for longer periods and a lower probability of getting hit by meteoroids [27].

Although lunar polar regions have many highly illuminated locations, there are high lunar terrain elevations as observed from the DEMs provided by the ongoing *Lunar Orbiter Laser Altimeter (LOLA)* experiment by NASA [30], [31]. The low solar elevation angles in the lunar polar regions and the high terrain create long shadows (in the range of kilometers) [21], [26], affecting the solar illumination on the polar sites. These shadows reduce the available power from the solar PV panels that can increase the PV and ESS requirements. At some locations, the required PV and ESS can be reduced by installing the PV panels on a tower, as shown in Fig. 1 [8]. There are some theoretical studies that show at some locations near the lunar North pole, installing a 100 m-tower can reduce the size of the required ESS size by 4%. The duration of ESS

TABLE 1. Some locations with high average solar illumination near the lunar south pole at a tower height of 10 m.

Site #	Longitude	Latitude	Average illumination (%)
1	222.6627	−89.4511	91.84
2	222.6415	−89.4333	85.09
3	222.8084	−89.4390	91.68
4	203.6490	−89.7797	86.90
5	203.2861	−89.7731	84.34
6	37.1013	−85.2963	78.84
7	123.7604	−88.8084	84.94
8	197.1382	−89.6866	86.18
9	222.4191	−89.4407	91.76
10	37.0207	−85.2897	82.44
11	291.7803	−88.6704	86.12
12	197.7447	−89.6884	80.18
13	202.8645	−89.7624	82.39
14	222.5634	−89.4734	87.87
15	222.7638	−89.4502	92.23

operation can be further reduced by 0.2 h/m by increasing the tower height to 300 m. It is shown that increasing the tower height to 1500 m and 3000 m near the lunar North and South pole, respectively, can eliminate the need for ESSs [21].

Table 1 presents the list of several locations with the highest average solar illumination near the lunar south pole [23], [24], [25]. Considering the Sun as a point source, the illumination profile time-series at Site #1 from July 6, 2023, to July 5, 2024 (1 year = 365.25 days × 24 hours = 8766 hours) at the height of 10 m is shown in Fig. 2. The solar illumination time-series at different sites can then be used to calculate the solar power generation profiles.

III. ESTIMATING PV POWER GENERATION

The high efficiency, radiation hardness, and mature manufacturing process make the multi-junction (MJ) PV cells based on III-V semiconductor technology a suitable choice for most of the space applications [8]. In a lunar base, despite having the advantage of the absence of an atmosphere, the power generation from the PV panels is dependent on the solar intensity, panel orientation, and inclination angle, among others [9].

The solar array output power can be calculated as follows [9]:

$$P^t_{PV} = (1 - \chi_d) f_{sc} \eta_{sc} A_a I_s \sin(\alpha + \beta) \tag{1}$$

where χ_d is the percentage of dust coverage, f_{sc} is the array fill factor, η_{sc} is the solar cell efficiency, A_a is the solar array area, I_s is the solar intensity, and α and β are the Sun elevation and PV array inclination angles, respectively. Due to the slight variation in the Earth and Moon system orbital eccentricity about the Sun, the solar intensity (I_s) on the Earth varies approximately from 1400 W/m^2 to 1308 W/m^2 [9]. However, I_s on the lunar surface varies slightly by a maximum of approximately 0.56% of that of Earth. This variation of I_s on the lunar surface is negligible, and thus the value of I_s on the Earth's orbit can be used. The vernal equinox with an I_s of 1359 W/m^2 [9] is considered for this study. To account for the effect of shadows on the available illumination at lunar sites, I_s is multiplied by the illumination time-series profile of the sites as shown in Fig. 2. Therefore, the shadowing effect due to the high lunar terrain elevations is considered while calculating P^t_{PV} in eq. 1.

TABLE 2. Parameters for calculating solar array output power.

Total number of hours in one lunar day (t_d)	708.33 hours
Total number of hours in one synodic day of the Earth	24 hours
Total number of Earth days in one tropical year (d_{nt})	365.25 days
Percentage of dust coverage (χ_d)	0
Solar cell fill factor (f_{sc})	0.89
Solar cell efficiency (η_{sc})	0.28
Maximum Moon declination angle (ψ_{max})	1.5

The Sun elevation angle (α) varies throughout the lunar day from sunrise to sunset at a given latitude as follows [9]:

$$\alpha = \frac{\pi}{2} - \cos^{-1}\left[\sin(\phi)\sin(\psi) - \cos(\phi)\cos(\psi)\cos\left(\frac{2\pi t_i}{t_d}\right)\right] \tag{2}$$

where ϕ is the lunar latitude, ψ is the lunar declination angle, t_i [h] is the instantaneous lunar daytime, and t_d [h] is the total hours in a lunar day. The lunar declination angle (ψ) is given by [9]:

$$\psi = \psi_{max} \sin\left(\frac{2\pi d_n}{d_{nt}}\right) \tag{3}$$

where d_n is the day number of the Earth and Moon system around the Sun and d_{nt} is the total number of days in one tropical year (days).

Different parameters used in this study to calculate α, ψ, and P^t_{PV} are listed in Table 2 [9]. As it is assumed that the lunar base camp has crew members and is located close to the power system infrastructures of the base, the solar arrays are considered to be regularly cleaned. Hence, χ_d is set to zero in this study. MJ GaInP/GaAs/Ge solar panels are widely used in space applications and have efficiencies of around 30% [32]. In this study, the solar array area (A_a) is a design parameter and is determined based on the power required by the lunar base.

Although the absence of an atmosphere is a boon for solar power generation on the Moon, the null atmosphere, along with weak magnetic fields, allows space debris and micrometeorites to reach the lunar surface. Moreover, ultraviolet, nuclei/ion particles, and cosmic radiations reach the solar cells, and electrostatic fields cause cell degradation [33]. Furthermore, the operating temperature of the PV cells affects the solar array's lifetime. The maximum operating temperature of the PV panels can be close to the surface temperature of $-193.15°C$ to $-163.15°C$ near the Shackleton crater [34], [35]. This severe temperature stress also reduces the lifetime of the PV cells. Several passive [36] and active [37] thermal control systems can be employed to keep the temperature

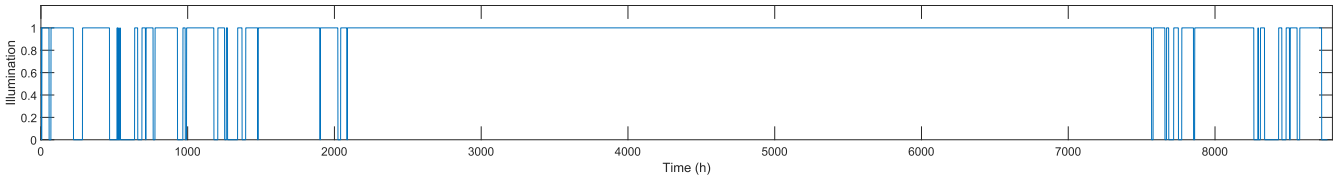

FIGURE 2. Illumination time-series profile at Site #1 from July 6, 2023, to July 5, 2024. Illumination "1" shows that the solar illumination is available at the location, and "0" indicates that the site is in shadow due to the low Sun elevation and high lunar terrain.

within the required operating range [38]. There are different studies related to the degradation of PV cells on low and medium Earth orbit spacecraft due to flux, fluence, intensity, and energy of particle radiations. However, studies related to particle radiations reaching the lunar surface and low lunar temperatures are scarce. Therefore, the degradation of PV cells on the Moon due to low temperature and particle radiation is yet to be thoroughly investigated and is not considered in this study.

IV. POWER CONSUMPTION UNITS OF SPACE MG

There can be different types of power consumption units (loads) in a lunar base depending on the space mission as shown in Table 3 [9], [10], [39]. The most probable load in a crewed mission is the lunar base habitat for the crew members consisting of LSSs for maintaining an artificial atmosphere with oxygen, heating, and cooling, maintaining food and water supplies, and running electrical equipment such as computers, communication instruments, lights, and displays. Additional LSSs' facilities may include waste processing and biomass composting units, contributing substantially to the overall habitat electrical power consumption [40]. In addition to the habitat, the base may consist of laboratories with various specialized equipment depending on the space mission [9] along with some loads similar to that of the habitat. Several remotely controlled or autonomous human or non-human carrying electric vehicles (EVs) may also be used to collect samples, transport, and perform maintenance tasks. Therefore, charging stations are required to charge the EVs [9], [10]. All different lunar establishments should be in constant communication with the habitat to monitor their vital parameters for the safe operation and security of the lunar base. This information should also be constantly communicated to the ground stations on Earth, which increases the need for electrical energy.

For extended periods of stay, ISRU is desired to be established to produce oxygen and propellants using the lunar regolith. The ISRU consists of an electrolyzer and several motors to scoop, filter, and transport the regolith that is in need of electrical energy to fulfill its functions. Additionally, thermal power is required for the catalyzed hydrogen reduction reaction of the regolith inside a boiler [9]. This thermal energy can be supplied from electrical heaters [9], further increasing the electrical energy demand. Alternatively, several researchers have proposed to utilize solar energy directly using solar concentrators and optical waveguides [41], [42], [43].

The lunar base loads can be divided into critical and non-critical loads. The non-critical loads can be switched off or put into a low-power (survival/idle) state during the lunar night and partial or total eclipses, and only critical loads are operated to reduce the size of ESSs. As summarized in Table 3, there might be similar loads in different sections of the lunar base. For example, *Air compressors* are required to maintain the artificial atmospheric pressure in all three sections of the base, namely habitat, laboratory, and ISRU. Instead of considering all the loads in a single MG, each section of the base can be considered as an MG with its local power production and ESS, creating an MMG system as shown in Fig. 3b. The total power required by the habitat depends on the number of crew members and is estimated to be around 10 to 30 kW for approximately 2 to 5 crew members [9], [10]. The power required by the ISRU can vary from tens to hundreds of kW for both thermal and electrical power and is dependent on the oxygen and propellant's production rate and process [9], [44]. Similarly, the power demands of different EVs and rovers depend on their range, energy storage capacities and self-discharge rate, lunar terrain, and the physical properties of the regolith [8], [10]. Communication systems can also have different power requirements depending on the frequency of communication, transmission rate and distance, and bandwidth [9]. The power required by the LSS may depend on the criticality of maintaining the artificial atmosphere, the rate of waste water filtration and so on. Therefore, different devices in Table 3 can consume varying power depending on the rate at which the device operates. In this paper, the power consumed by different power-consuming units is assumed to be constant during their time of use.

A. LOAD PROFILE GENERATION AND ANALYSIS

The load profile for each site listed in Table 1 is generated considering the solar power generation profiles of the sites and the time of use of different loads according to Table 3 [10], [39]. The active-state power demand of all loads are summed for each hour over 24 hours when the solar power is available on the site. At the time when the solar power is not available, only the survival-state power demand of critical loads are taken into account. The power consumption of loads at each hour (P_L^t) is calculated as

TABLE 3. Specifications of several power consuming units in different sections (Habitat (H), Laboratory (L), and ISRU (I)) of a lunar base.

Section			Device	Active-state power (W)	Survival-state power (W)	Average daily use (h)	Time of use (h)
H	L	I	Air compressor	3.5	3.5	24	0 - 24
H	L	I	Airlock vacuum pump	500	500	1	21 - 22
H	L	I	Airlock status LED	5	5	24	0 - 24
H	L	I	Artificial daylight LED	150	75	24	0 - 24
H			Water heater	4000	0	1	6 - 7
H			LSS	4500	3000	24	0 - 24
H			Induction oven	2000	0	1	8 - 9
H	L	I	Monitoring camera (9 Nos)	5	5	24	0 - 24
H	L		Laptop	60	60	12	9 - 21
H	L	I	LCD display	160	0	24	0 - 24
H	L	I	Lighting LED lamps (33 Nos)	20	10	4	20 - 24
H			Microwave	800	0	2	7 - 9
H	L		Projector	60	0	1	10 - 11
H			Crew Laptop-1	65	0	10	8 - 18
H			Crew Laptop-2	80	0	6	9 - 15
H			Crew Laptop-3	60	0	3	9 - 12
H			Crew Laptop-4	80	0	10	9 - 19
H			Crew Laptop-5	65	0	8	9 - 17
H			Crew Laptop-6	70	0	2	18 - 20
H			Crew Smartphone-1	2	0	1	19 - 20
H			Crew Smartphone-2	2	0	1	20 - 21
H			Crew Smartphone-3	5	0	2	20 - 22
H			Crew Smartphone-4	3	0	2	17 - 19
H			Crew Smartphone-5	2	0	3	18 - 21
H			Crew Smartphone-6	3	0	1	20 - 21
H	L		Camera-1	10	0	2	10 - 12
H	L		Camera-2	10	0	1	15 - 16
H	L		Camera-3	10	0	1	21 - 22
H			Treadmill	800	0	5	5 - 10
H	L		Refrigerator	10	10	24	0 - 24
H			Hair dryer	1200	0	1	8 - 9
H			Washing machine	2000	0	1	18 - 19
H			Vacuum cleaner	1.5	0	1	7 - 8
H	L	I	Electrical power system	200	200	24	0 - 24
H	L	I	Communication system internal components	1500	750	24	0 - 24
H	L	I	Communication system external components	1000	1000	24	0 - 24
H	L	I	Central computer	100	100	24	0 - 24
H	L		Spacesuit battery charger	140	140	6	23 - 5
H	L		Sample drill battery charger	2000	0	1	15 - 16
H	L	I	Lunar day active thermal control system	1200	900	24	0 - 24
H	L	I	Lunar night active thermal control system	1900	1500	24	0 - 24
H	L	I	Sensors	4000	3000	24	0 - 24
	L		3D printer	700	0	12	9 - 21
	L		Welder	5000	0	1	11 - 12
	L		Laboratory electric arc furnace	5000	0	1	13 - 14
	L		Manufacturing device	2000	0	1	10 - 11
	L		Rover charging	7000	1000	6	23 - 5
	L		Pressurized EV charging	10 000	3000	6	23 - 5
	L		Unpressurized EV charging	3000	2000	6	23 - 5
		I	ISRU	65 000	500	24	0 - 24

follows:

$$P_L^t = \begin{cases} \sum_{u=1}^{U} P_u^a(t) & P_{PV}^t > 0 \\ \sum_{u=1}^{U} P_u^s(t) & P_{PV}^t = 0 \end{cases} \tag{4}$$

where u is a power consumption unit, U is related to the set of power consuming units, and P_u^a and P_u^s are the active-state and survival-state power of each unit u at time t. Similarly, the load profile for each section, namely habitat, laboratory, and ISRU can be created.

V. BATTERY SIZING AND OPTIMIZATION

In this section, the optimization problem to determine the optimal size of the battery and PV is introduced. The goal is to minimize the mass of the battery and PV system as well as the battery cost. Besides, there are several technical and operational constraints that must be met.

A. BATTERY CONSTRAINTS

There are different types of ESSs that can be used in space applications. According to [45], ESSs with energy density of ~500 Wh/l, specific energy of ~250 Wh/kg, calendar life of

~5 years, cycle life of ~1000 cycles, radiation tolerance, and low temperature (~−40°C) operational capability are desired for space surface missions. ESSs with high specific energy and energy density have lower mass and volume, respectively. Different types of ESSs such as primary (non-rechargeable) and secondary (rechargeable) batteries, fuel cells (FCs), capacitors, and flywheels are used in space missions [45], [46]. Utilization of different types of ESSs depends on their time of use as well as the mission purposes. Among these, rechargeable batteries and FCs have the desired specifications to support the loads for long hours [45]. Lithium-ion (Li-ion) batteries have high specific energy (~150−200 Wh/kg) and energy density (more than 200 Wh/l) compared to other rechargeable batteries [9], [45], [46]. Moreover, the charging efficiency of batteries is higher than RFCs, which reduces the required time to recharge them [22]. A more detailed comparison of RFCs and rechargeable batteries can be found in [8]. Considering the advantages and abundant use of Li-ion batteries for space applications, the sites are considered to be equipped with Li-ion batteries in this study.

Different sites on the Moon have various illumination conditions that affect the size of the required batteries. Depending on the mismatch between solar power generation and the power demand, the batteries are charged and discharged. The charging and discharging equations of the battery are given by:

$$\begin{aligned} \text{Charging: } E(t+1) &= E(t) + P_c^t \eta_c \Delta t \\ \text{Discharging: } E(t+1) &= E(t) - \frac{P_d^t}{\eta_d} \Delta t \end{aligned} \tag{5}$$

where $E(t)$ is the battery energy at time instant t, P_c^t and P_d^t are battery charging and discharging power, η_c and η_d are battery charging and discharging efficiencies, and Δt is the time between two instants. Here, P_c^t and P_d^t are limited by:

$$\begin{aligned} 0 \le P_c^t &\le P_c^{t,max} \\ 0 \le P_d^t &\le P_{d,}^{t,max} \end{aligned} \tag{6}$$

where $P_c^{t,max}$ and $P_d^{t,max}$ are the maximum power for charging and discharging the battery. The stored energy in the battery is limited by:

$$E^{min} \le E(t) \le E^{max} \tag{7}$$

where E^{min} and E^{max} are the minimum and maximum allowable energy of the battery. In this study, E^{min} and E^{max} of the battery are defined as:

$$\begin{aligned} E^{min} &= (1 - B_{dod})\, E_{cap} \\ E^{max} &= B^{max} E_{cap} \end{aligned} \tag{8}$$

where B_{dod} and B^{max} are the battery depth of discharge (DOD) and maximum charge, respectively, and E_{cap} is the battery capacity. The battery energy at the end of the optimization horizon (T) is limited by:

$$E(T) = (1 \pm \delta) E(0) \tag{9}$$

where $E(0)$ and $E(T)$ are the battery energy at the start and end of the optimization horizon, and δ has a value between 0 and 1 to introduce a soft constraint on the final energy condition of the battery.

The initial establishment of the lunar base can be considered as an islanded MG as there are no other MGs or a central grid. Therefore, the excess PV energy is stored in the batteries while the stored energy is used to supply the loads when the energy generation is not enough to cover the power demand. The minimum energy charged $\left(E_c^{min}\right)$ and discharged $\left(E_d^{min}\right)$ to and from the batteries are given by:

$$\begin{aligned} E_c^{min} &= \int_0^T \left(P_{PV}^{t,min} - P_L^t\right) \delta t;\; P_{PV}^{t,min} > P_L^t \\ E_d^{min} &= \int_0^T \left(P_L^t - P_{PV}^{t,max}\right) \delta t;\; P_L^t > P_{PV}^{t,max} \end{aligned} \tag{10}$$

where $P_{PV}^{t,min}$ and $P_{PV}^{t,max}$ are the minimum and maximum PV power generation at hour t, and T is the total number of hours in the optimization horizon. Thus, the minimum energy stored in the battery $\left(E_B^{min}\right)$ can be calculated as follows [47]:

$$E_B^{min} = \max\left(\eta_c E_c^{min}, \frac{E_d^{min}}{\eta_d}\right) \tag{11}$$

In this paper, E_B^{min} is used as the initial guess for the battery size in the optimization problem.

B. BATTERY DEGRADATION

Li-ion battery degradation depends on several factors such as charging and discharging cycles, stress due to temperature, state-of-charge (SOC), and time. Charging and discharging cycles cause cyclic aging in batteries resulting in loss of battery life and capacity fading [48]. Apart from that, the inherent degradation in batteries over time is given by calendar aging [48]. The cyclic aging $\left(L_{cyc}\right)$, calendar aging (L_{cal}), and total capacity fade (f_d) models proposed in [48] are given below:

$$\begin{aligned} L_{cyc} &= \sum_i^N n_i f_{cyc}\left(\rho_i, \lambda_i, T_{c,i}\right) \\ L_{cal} &= f_{cal}\left(t, \overline{\rho}, \overline{T}_c\right) \\ f_d &= L_{cyc} + L_{cal} \end{aligned} \tag{12}$$

where N is the number of cycles, n_i denotes if the i^{th} cycle is a half cycle ($n_i = 0.5$) or full cycle ($n_i = 1$), ρ_i is the average SOC of the i^{th} cycle, λ_i is the DOD of the i^{th} cycle, $T_{c,i}$ is the average cell temperature of the i^{th} cycle, t is time instant, $\overline{\rho}$ is the average SOC, and $\overline{T}_c$ is the average cell temperature. The cyclic and calendar degradation is further dependent on the stress due to the battery SOC $\left(S_\rho\right)$, DOD (S_λ), cell temperature (S_T), and time period (S_t) as follows:

$$\begin{aligned} f_{cyc}(\rho, \lambda, T) &= S_\lambda(\lambda) S_\rho(\rho) S_T(T) \\ f_{cal}(t, \rho, T) &= S_t(t) S_\rho(\rho) S_T(T). \end{aligned} \tag{13}$$

TABLE 4. Degradation model parameters.

Degradation coefficients	Value	Degradation coefficients	Value
$k_{\lambda 1}$	1.40×10^{5}	ρ_{ref}	0.5
$k_{\lambda 2}$	-5.01×10^{-1}	k_T	6.93×10^{-2}
$k_{\lambda 2}$	-1.23×10^{5}	T_{ref}	$25°C$
k_ρ	1.04	k_t	$4.14 \times 10^{-10} s^{-1}$

The stress factors S_λ, S_ρ, S_T, and S_t are given below:

$$S_\lambda(\lambda) = \left(k_{\lambda 1}\lambda^{k_{\lambda 2}} + k_{\lambda 3}\right)^{-1} \tag{14}$$

where $k_{\lambda 1}$, $k_{\lambda 2}$, and $k_{\lambda 3}$ are the battery DOD coefficients.

$$S_\rho(\rho) = e^{k_\rho(\rho - \rho_{ref})} \tag{15}$$

where k_ρ is the SOC stress coefficient and ρ_{ref} is the reference SOC level (usually around 0.4 to 0.5).

$$S_T(T) = e^{k_T(T - T_{ref})\frac{T_{ref}}{T}} \tag{16}$$

where k_T is the temperature stress coefficient and T_{ref} is the reference temperature ($25°C$).

$$S_t(t) = k_t t \tag{17}$$

where k_t is the calendar time stress coefficient. Different degradation model parameters used in this study are given in Table 4 [48].

The battery cycles and fatigue were determined using the widely used *Rainflow* cycle-counting algorithm [48]. This algorithm takes the battery SOC as input and calculates the cycle number (0.5 for half cycle and 1 for full cycle), DOD of the i^{th} cycle, average SOC of the i^{th} cycle, and cycle starting and end times. The temperature near the Shackleton crater is around $--193.15°C$ to $-163.15°C$ [34], [35], which is much lower than the operating temperatures of the batteries. Using the active and passive thermal control systems, the cell temperature is assumed to be kept around the operating temperature of $22°C$. Therefore, the loss in capacity of the battery is calculated as:

$$E_{cap}^{new} = (1 - f_d)\, E_{cap} \tag{18}$$

where E_{cap}^{new} is the new reduced capacity of the battery. Furthermore, there is a constraint for the number of battery cycles, which is a critical degradation indicator for Li-ion batteries, as follows:

$$B_{cycles} < B_{totcycles} \tag{19}$$

where $B_{totcycles}$ is the total number of battery cycles that depends on the battery DOD (B_{dod}) as [9]:

$$\begin{aligned} B_{totcycles} = {} & -0.0799\, B_{dod}^3 + 20.035\, B_{dod}^2 \\ & - 1757.6\, B_{dod} + 57778 \end{aligned} \tag{20}$$

and B_{cycles} can be calculated from the output of the Rainflow cycle-counting algorithm.

Algorithm 1 Battery Capacity and PV Array Area Optimization

1: Calculate illumination time series considering the Sun, Earth, and Moon three-body system
2: Estimate PV power generation using (1)-(3)
3: Generate load profile using Table 3 and (4)
4: Calculate E_B^{min} using (10)-(11)
5: Solve the optimization problem to minimize (22) using (23)-(26) subject to constraints (5)-(9) and (12)-(21)

For space applications, cosmic and particle radiation is also an important factor for battery degradation. Although, in many applications, proper shielding can be employed to protect the batteries from the harsh environment and harmful radiation, complete protection can never be assured. There are several data-driven models for Li-ion battery degradation for spacecraft in low and medium-altitude Earth orbits. These studies rely on the data collected by spacecraft and are mostly specific to limited areas of application. Moreover, there are studies dedicated to other factors of battery degradation, such as battery electrodes and electrolytes. Therefore, battery degradation due to space radiation on the lunar surface still needs to be explored and is out of the scope of this study.

C. POWER BALANCE CONSTRAINT

The hourly real power balance is considered as:

$$P_{PV}^t = P_L^t + P_B^t \tag{21}$$

where P_{PV}^t and P_B^t are the PV and battery power at each hour, respectively, and $P_B^t = P_c^t$ for charging while $P_B^t = -P_d^t$ for discharging.

D. OPTIMAL SIZING ALGORITHM

Establishing a lunar base involves costly space missions to transport different equipment to the Moon. The cost of space missions is directly proportional to the payload mass along with other critical factors such as equipment size and stowage area. In this study, the size of the PV array and battery mass along with the total cost per day (TCPD) of the battery are considered as optimization goals to be minimized. The PV array and battery are some of the critical components of the electrical power system of the lunar base and are among the heavy electrical structures for transportation. In this study, the following objective function is proposed to minimize to size of the PV array and battery mass as well as TCPD of the battery:

$$\begin{aligned} J(E_{cap}, A_a) = {} & TCPD(r, l, E_{cap}, MC, FC) \\ & + M_B(E_{cap}) + M_{PV}(A_a) \end{aligned} \tag{22}$$

where r is the interest rate for financing the installed battery, l is the battery lifetime, MC is the battery maintenance cost in \$/kWh, FC is the first time battery cost in \$/kWh, $M_B(E_{cap})$ is the battery mass, and M_{PV} is the PV mass as a function of the PV array area (A_a). The TCPD of the battery is considered

as follows [47]:

$$TCPD = \frac{1}{365}\left(AOTC(r, l, E_{cap}, FC) + E_{cap} \times MC\right) \quad (23)$$

where the annualized one-time ESS cost (AOTC) is given below:

$$AOTC = \frac{r(1+r)^l}{(1+r)^l - 1} FC \times E_{cap} \quad (24)$$

The battery mass in eq. 22 is [9]:

$$M_B = \frac{E_{cap}}{S_b B_{dod}} \quad (25)$$

where S_b is the battery specific energy, which is considered 200 Wh/kg according to [9]. Finally, the PV mass in eq. 22 is calculated as follows [9]:

$$M_{PV} = \sigma_s A_a \quad (26)$$

where σ_s is the solar array structure specific mass set to 0.55 kg/m^2 following [9].

It is vital to maintain the power balance in the system while minimizing the space mission cost. The optimization problem aims at minimizing the objective function in eq. 22 to minimize M_{PV}, M_B, and the battery $TCPD$. All the constraints related to the physical operation of the battery, as presented in the previous subsections, have been included in the optimization problem formulation. Decision variables are E_{cap} and A_a that needs to be determined to minimize M_B, M_{PV}, and the battery TCPD using eq. 25, eq. 26, and eq. 23, respectively. The optimal sizing of A_a ensures that the power demand is supplied and the battery is charged before the duration when solar energy is not available without generating excess power than required. An overview of the proposed optimization procedure is presented in Algorithm 1.

VI. RESULTS

In this study, the optimal size for the battery and PV are calculated for a number of highly illuminated candidate sites near the lunar south pole, Shackleton crater. The non-linear optimization problem has been implemented in MATLAB R2020b, and *fmincon* solver has been chosen to solve the problem using the 'interior-point' algorithm. Two optimization horizons of 1 year and 5 years have been considered for optimal siting and sizing of the lunar base. Battery capacity degradation is only considered in the case with 5 years optimization horizon. Battery cost data and other parameters used for simulation are given in Table 5 [9], [47]. E^{max} and E^{min} are set to 90% and 20% of the total battery capacity (E_{cap}), respectively. The PV arrays are considered to be placed on top of towers with heights of 10, 50, and 100 m.

As discussed in Section IV, the power system for the lunar base can be designed as an MMG system or a single MG. In the following, both cases are investigated and discussed.

TABLE 5. Battery parameters.

Battery parameters	Value
r	6%
l	1 (for 1 year optimization horizon) 5 (for 5 year optimization horizon)
FC	600 \$/kWh
MC	20 \$/kWh
B_{dod}	80 %
η_c	80 %
η_d	80 %

A. CASE 1: THE SINGLE MG DESIGN

In this case, the power system is considered as a single MG with aggregated PV and battery storage systems as shown in Fig. 3a. Implementing the proposed optimization algorithm, results for the battery energy state, PV array generation profile, power demand, and battery charging and discharging patterns for Site #2 for the optimization horizons of 1 year (= 8766 h) and 5 years (= 43830 h) are shown in Fig. 4a and Fig. 4b, respectively. The PV generation profile is estimated using the methodology described in Section III considering the arrays installed on 10 m high towers and with PV array area (A_a) of 303.83 m^2 and 304.97 m^2 for 1 year and 5 years optimization horizon respectively, obtained from the optimization algorithm. As discussed in Section IV, it can be seen from Fig. 4 that the power demand drops to the survival-state when the solar power is unavailable, and the power demand is supplied from the battery. As shown in Fig. 4b, the maximum and minimum battery energy capacity reduces after each year for 5-year simulation horizon due to the battery calendar and cyclic aging as discussed in Section V.

For different sites from #1 to #15, the optimized battery capacity (in Wh) and mass (in kg) are in the order of 10^7 and 10^5, respectively, for both 1 year and 5 years optimization horizon as shown in Fig. 5a, Fig. 5b, Fig. 6a, and Fig. 6b. Both the PV array area (in m^2) and mass (in kg) are in the order of 10^2 for both 1-year and 5-year optimization horizons as shown in Fig. 5c, Fig. 5d, Fig. 6c, and Fig. 6d. Also, no significant change in the PV array area and mass are observed when the optimization horizon is increased from 1 year to 5 years due to neglecting PV degradation. The total system mass is then calculated by adding the battery mass and the mass of PV array as shown in Fig. 9a and Fig. 9b for 1 year and 5 years optimization horizons, respectively.

Increasing the tower height from 10 m to 50 and 100 m reduces the shadowing effect on the sites caused by the high terrain at the lunar polar regions. Therefore, increasing the tower height increases the average illumination as shown in Fig. 10a. As the illumination increases, the longest darkness period of the sites reduces, as can be seen from Fig. 10b. Increasing the tower height from 10 m to 50 m increases the average illumination approximately from 84% to 92% for Site #2 and from 78% to 87% for Site #12. A similar significant increase in the illumination condition is also

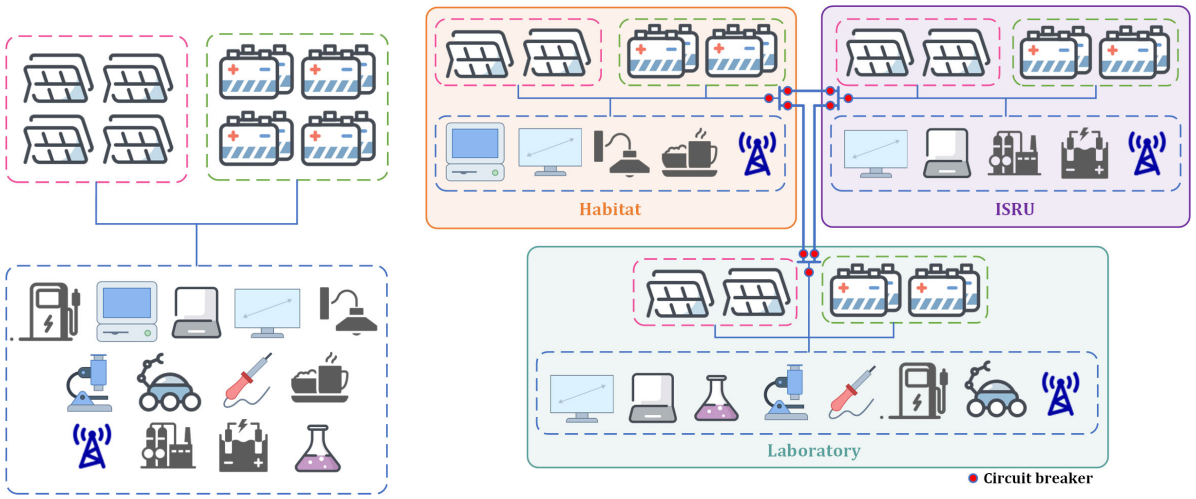

(a) Case 1: The single MG design (b) Case 2: The MMG system design

FIGURE 3. Two different design approaches for the lunar base power system.[1]

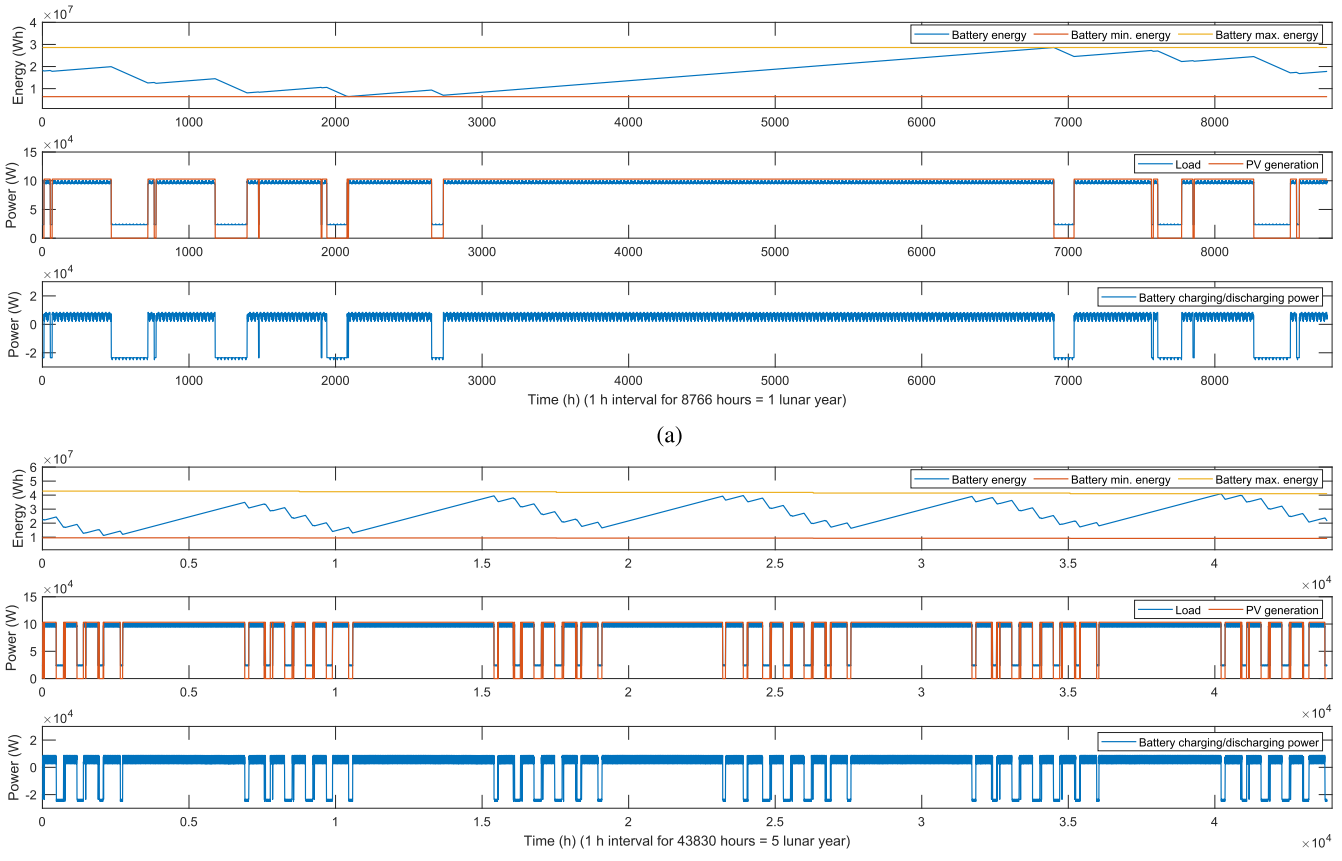

(a)

(b)

FIGURE 4. Battery energy state, PV and power demand, and battery charging and discharging power profiles for Site #2 and the single MG case with PV array installed at 10-m tower height for (a) 1 year without considering battery degradation (b) 5 years considering battery capacity degradation.

observed in Sites #6, #13, and #14. It should also be noted that the illumination condition and the longest continuous nights are different during the 5 years, and optimization results for one year may be close to the results of other years but not exactly the same. A similar observation is reported in [22]. The longest continuous night for all sites reduces with an increase in the tower height. The increase in average illumination and decrease in darkness period reduce the duration for which the power demand is supplied from the batteries, thereby reducing the battery size and mass as

[1]https://icons8.com

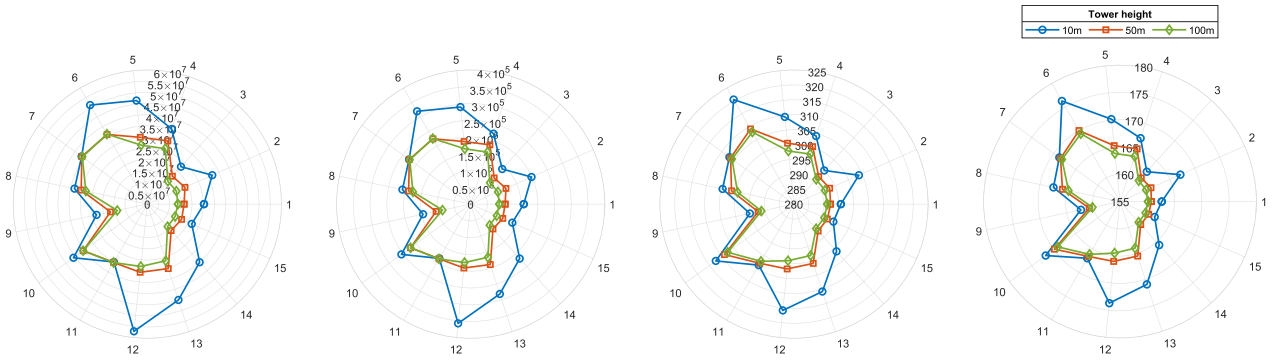

(a) Battery size (in Wh) (b) Battery mass (in kg) (c) PV array area (in m^2) (d) PV array mass (in kg)

FIGURE 5. Battery and PV array size and mass for the 1-year optimization horizon for the single MG case without battery capacity degradation at different tower heights.

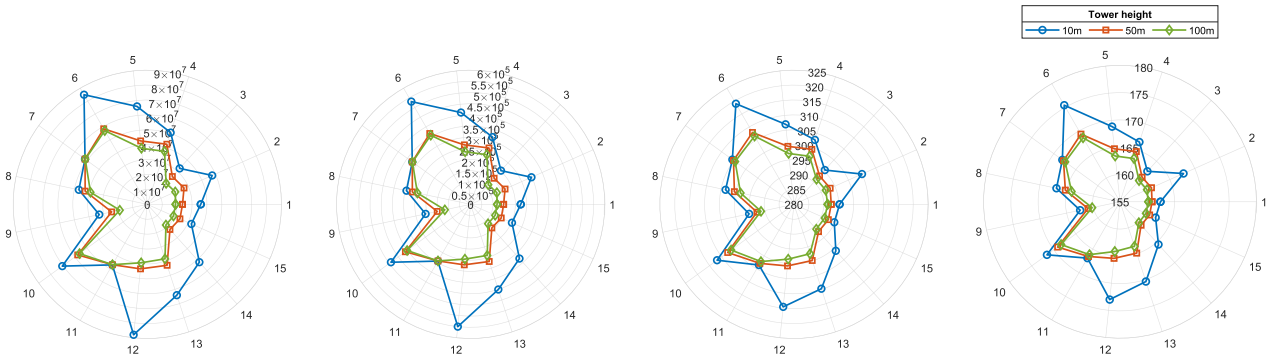

(a) Battery size (in Wh) (b) Battery mass (in kg) (c) PV array area (in m^2) (d) PV array mass (in kg)

FIGURE 6. Battery and PV array size and mass for the 5-year optimization horizon for the single MG case with battery capacity degradation at different tower heights.

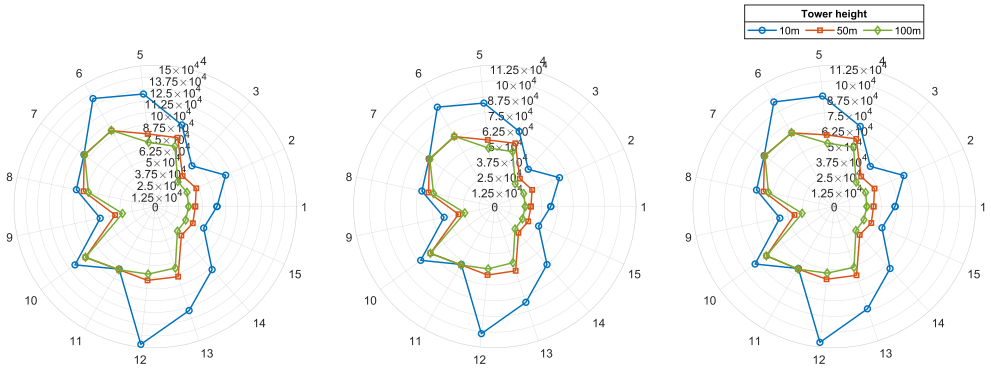

(a) Habitat (b) Laboratory (c) ISRU

FIGURE 7. Total mass (in kg) of battery and PV for different sections of MMG system for the 1-year optimization horizon without considering battery capacity degradation at different tower heights.

can be seen in Fig. 5a, Fig. 6a, Fig. 5b, and Fig. 6b. The decrease in the total mass of the system with an increase in the tower height can be observed in the case of single MG in Fig. 9a and Fig. 9b. Although increasing the tower height will increase the tower mass, the battery mass also reduces in the order of 10^5 kg. Moreover, as discussed in [49], tall towers on the Moon can also be used for other purposes such as lighting, long-distance communication, and power transmission using microwaves or lasers. The authors also discuss the possibility of constructing concrete towers as concrete can be produced on-site from lunar regolith. Therefore, the cost of transporting the towers from the Earth can be saved. Other than concrete, a tower frame made up of metal trusses can also be investigated to reduce the mass of the tower. Also, there are proposals from space agencies to construct autonomously deployable and retractable 32-feet ($\sim$ 9.75 m) high towers for solar array systems [50]. From Fig. 10a, it can be observed that for Sites #2, #5 #6,

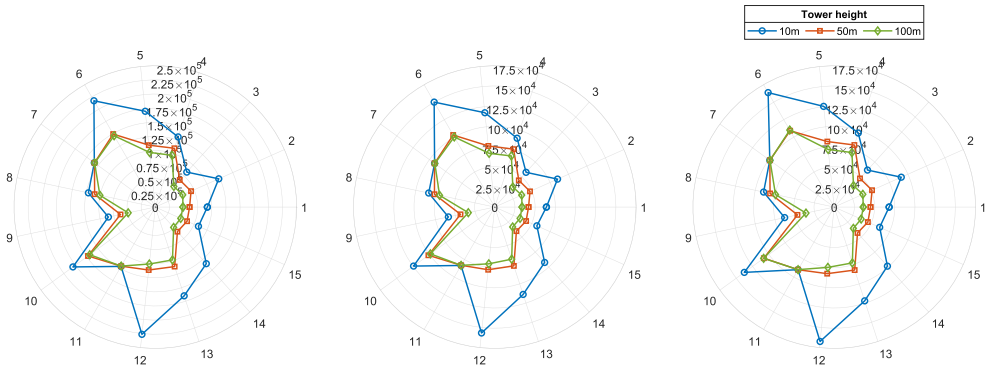

(a) Habitat (b) Laboratory (c) ISRU

FIGURE 8. Total mass (in kg) of battery and PV for different sections of MMG system for the 5-year optimization horizon considering battery capacity degradation at different tower heights.

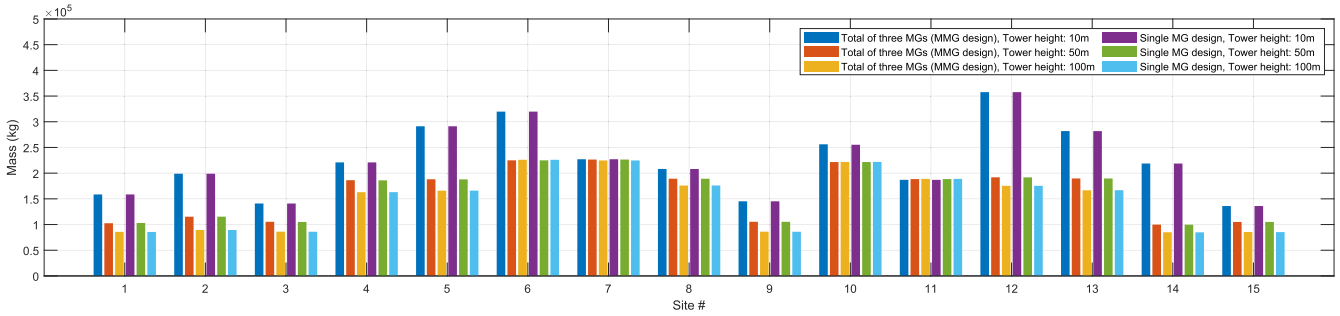

(a) Total mass of three MGs and single MG system for the 1-year optimization horizon

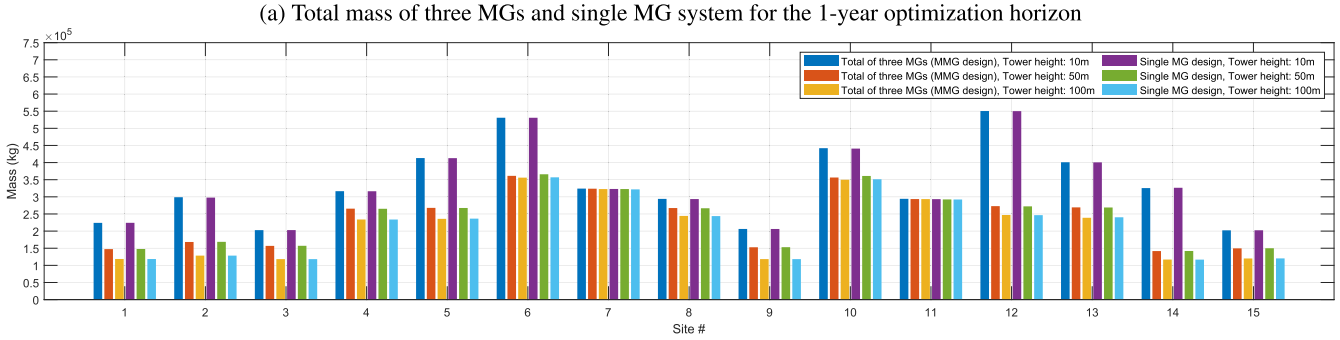

(b) Total mass of three MGs and single MG system for the 5-year optimization horizon

FIGURE 9. Total battery and PV mass comparison for the 1-year optimization horizon without considering battery capacity degradation and 5-year optimization horizon considering yearly battery capacity degradation at different tower heights.

#12, #13, and #14 increasing the tower height from 10 m to 50 m and 100 m increases the illumination significantly. Hence, a considerable change in the total system mass can be observed in Fig. 9a and Fig. 9b in these sites. At Site #12, increasing the tower height to 50 m or 100 m reduces the total system mass from 3.57×10^5 kg to approximately 1.9×10^5 kg and from 5.5×10^5 kg to approximately 2.5×10^5 kg for the 1-year and 5-year optimization horizons, respectively. At Sites #2 and #14, increasing the tower height from 10 m to 50 m reduces the total system mass to approximately half of the total system mass with a 10 m-tower height for both 1-year and 5-year optimization horizons. Comparing the sites in Fig. 10, Sites #1, #3, #9, and #15 are the most illuminated sites and have the lowest total mass. On the other hand, Sites #6, #7, and #10 have the lowest average illumination and are among the sites with the longest continuous night hours and, therefore, have the highest total system mass. Interestingly, there is not much change in the illumination with the increase in the tower height for Sites #7 and #11. Therefore, the total system mass for Sites #7 and #11 does not change considerably with the increase in the tower height.

B. CASE 2: THE MMG DESIGN

In the case of a single MG, due to the centralized power generation system and control, the risk of a single point of failure can threaten the system stability, thus reducing the reliability of the system. Besides, considering the cost and criticality of space missions, it might not always be possible to have expert crews on board. Thus, an autonomous, highly

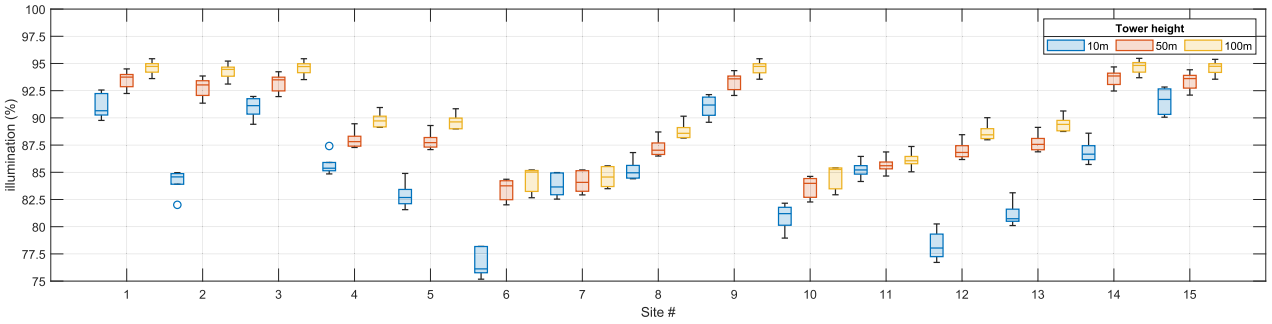

(a) Illumination condition for all sites during 5 years

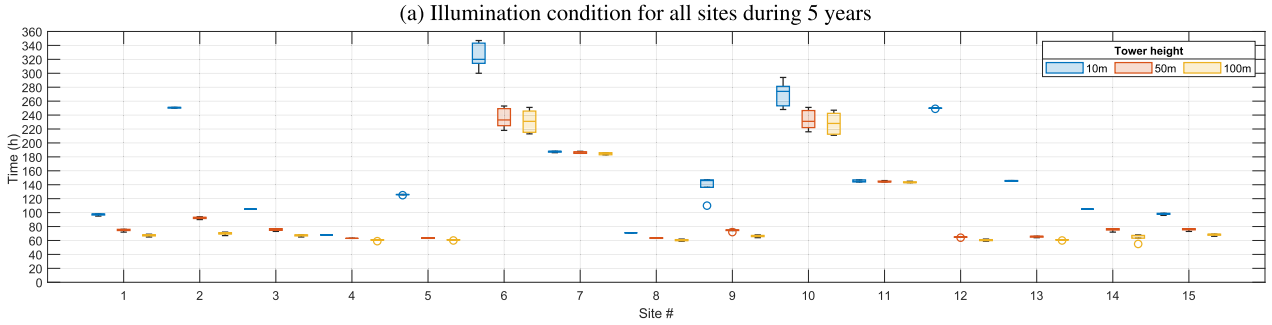

(b) Longest continuous night for all sites during 5 years

FIGURE 10. **Illumination condition at different tower heights.**

robust, and reliable power system is desired. The MMG system, as shown in Fig. 3b, can benefit from power sharing among different MGs in case of any disturbance or faults. Therefore, the reliability of the whole power system will increase. In this case, an MMG system is designed for the lunar base with three MGs for habitat, laboratory, and ISRU, as shown in Fig. 3. The total system mass for the three MGs at different sites are shown in Fig. 7 and Fig. 8 for 1-year and 5-year optimization horizons, respectively. The total system mass of the MMG system consisting of the mass of the three MGs together at different sites are shown in Fig. 9a and Fig. 9b for 1-year and 5-year optimization horizons, respectively. It can be seen that the total system mass of the MMG system also reduces as the tower height increases, as observed in the case of single MG. According to the results, the total system mass of the MMG system (considering *only* the mass of required batteries and PV arrays for each MG) is almost the same as the mass of the single MG for all sites and for both the 1-year and 5-year optimization horizons. Therefore, it can be concluded that the reliability of the power system can be increased by the MMG design without increasing the total PV-ESS system mass. However, the total mass for the case of MMG design is expected to be higher considering the extra mass of other required equipment such as cables, power converters, protection systems, etc. Thus, a more detailed analysis is needed that is the subject of the future study of the authors.

To have a fair comparison between different candidate sites, apart from the total system mass, the total power demand that is served at these sites should also be considered. The maximum and average power demand served in both single MG and MMG cases using the active and survival-state power demand represented in Table 3 is shown in Table 6. The daytime average power demand of the base depends on the active-state power of the power-consuming units, while the nighttime average depends on the survival-state power demand. The daytime $P_{L_d}^{avg}$ and nighttime average power demand $P_{L_n}^{avg}$ of the base is given by:

$$P_{L_d}^{avg} = \frac{\sum_{t=0}^{T_d} P_L^t}{T_d}$$
$$P_{L_n}^{avg} = \frac{\sum_{t=0}^{T_n} P_L^t}{T_n} \tag{27}$$

where T_d and T_n are the total number of day and night hours, respectively. The peak-to-average ratio (PAR) of the load at the day $P_{L_d}^{PAR}$ and night $P_{L_n}^{PAR}$ hours is given by:

$$P_{L_d}^{PAR} = \frac{\max P_L^{t_d}}{P_{L_d}^{avg}}$$
$$P_{L_n}^{PAR} = \frac{\max P_L^{t_n}}{P_{L_n}^{avg}} \tag{28}$$

where $P_L^{t_d}$ and $P_L^{t_n}$ are the load power at each hour during the day and night, respectively. In this paper, to select the best site for establishing the lunar base, a criterion based on the total power demand served at a site, and the corresponding total system mass is introduced. The total power demand served at

TABLE 6. Daytime and nighttime maximum and average power demand.

Power consuming units	Daytime power demand (W)			Nighttime power demand (W)		
	Peak	Average	PAR	Peak	Average	PAR
Habitat	1.77×10^4	1.37×10^4	1.29	1.01×10^4	9.70×10^3	1.04
Laboratory	1.41×10^4	9.32×10^3	1.51	7.15×10^3	6.70×10^3	1.06
ISRU	7.38×10^4	7.33×10^4	1.00	7.64×10^3	7.16×10^3	1.06
Single MG design	1.00×10^5	9.63×10^4	1.04	2.49×10^4	2.35×10^4	1.06

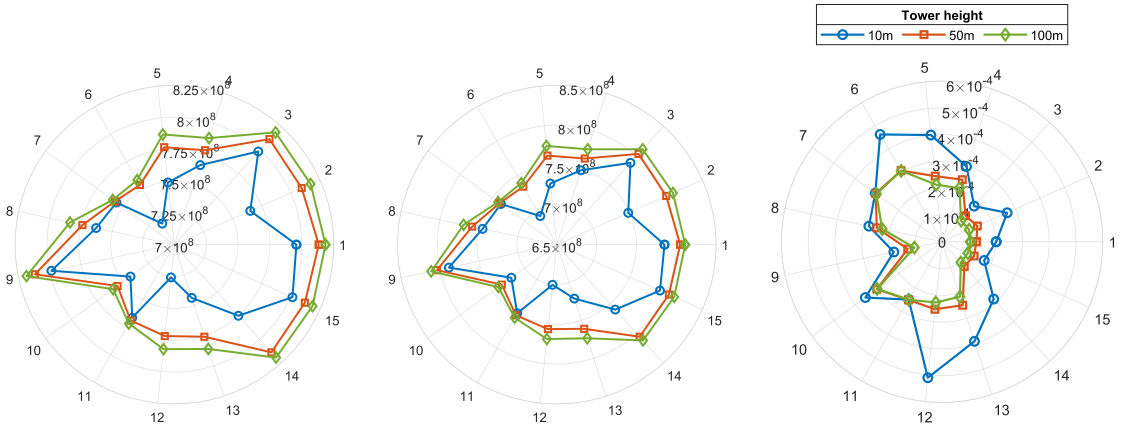

(a) Total PV power generation (in W) (b) Total power demand (in W) (c) Ratio of total mass to total power demand served (in kg/W)

FIGURE 11. PV generation, total power demand, and total mass to total power demand ratio for the 1-year optimization horizon for the single MG case at different tower heights.

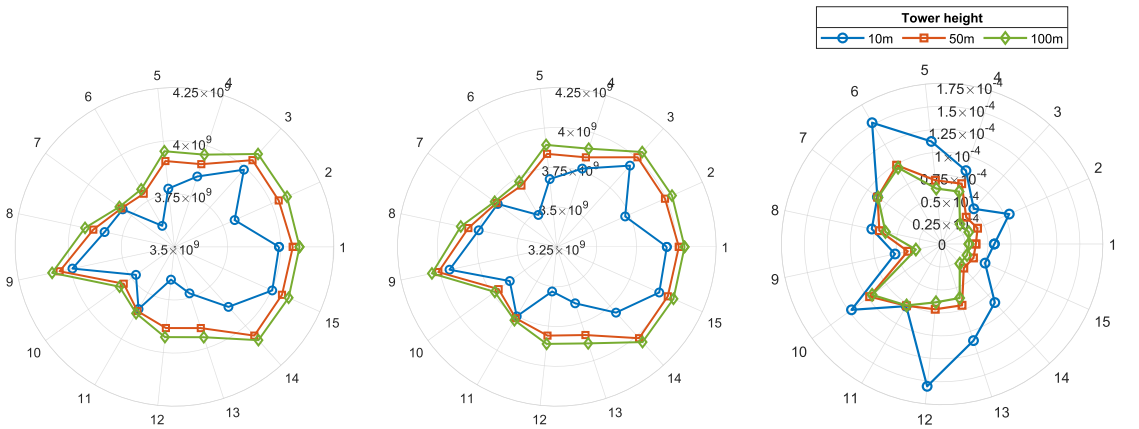

(a) Total PV power generation (in W) (b) Total power demand (in W) (c) Ratio of total mass to total power demand served (in kg/W)

FIGURE 12. PV generation, total power demand and total mass to total power demand ratio for the 5-year optimization horizon for the single MG case at different tower heights.

the site is given by:

$$P_L^{total} = \sum_{t=0}^{T} P_L^t \tag{29}$$

where T is the total number of hours in the optimization horizon. Then, the ratio of the total system mass to total power demand served at each site is called as mass-per-unit-load (MPUL) and is calculated as follows:

$$\text{MPUL} = \frac{\text{Total system mass}}{P_L^{total}} \tag{30}$$

The total PV array power generation, total power demand, and the MPUL ratio for 1-year and 5-year optimization horizons for each site are shown in Fig. 11 and Fig. 12, respectively. The sites with the least MPUL are desired as they can serve more power demand with less total system mass. It is observed from Fig. 11b and Fig. 12b that Sites #1, #3, #9, and #15 serve the highest power demand with 10-m tower height for both 1-year and 5-year optimization horizons, which is approximately 7.8×10^8 W and 3.9×10^9 W, respectively. However, Sites #3 and #15 have the least MPUL among them for both 1-year and 5-year optimization

horizons, which is approximately 1.7×10^{-4} kg/W and 5.1×10^{-5} kg/W, respectively. If the tower height is increased to 50 m, Sites #1, #2, #3, #9, #14, and #15 have a low similar MPUL of approximately 1.3×10^{-4} kg/W for 1-year optimization horizon and Site #14 has the least MPUL of 1.2375×10^{-4} kg/W. For the 5-year optimization horizon and with 50 m tower height, Sites #1, #14, and #15 have approximately similar MPUL of almost 3.6×10^{-5} kg/W and Site #14 has the least MPUL of 3.53×10^{-5} kg/W. With increasing the tower height to 100 m, Site #1, #3, #9, #14, and #15 have a low similar MPUL of approximately 1.05×10^{-4} kg/W and 2.9×10^{-5} kg/W, respectively for both 1-year and 5-year optimization horizons. Among these, Site #14 has the least MPUL of 1.0446×10^{-4} kg/W for 1-year and 2.879×10^{-5} kg/W for 5-year optimization horizon.

VII. CONCLUSION

This study was dedicated to optimal sizing and siting of a PV/battery space MG considering the battery storage system cost and mass, as well as the mass of PV arrays. Highly accurate solar illumination time-series were used to estimate the PV power generation profile at 15 highly illuminated candidate sites considering the PV arrays on towers with different heights of 10, 50, and 100 m. Power demand profiles of different power-consuming units in a lunar base and their time of use were identified. The PV power generation profile along with the information of the power demand, were used to optimally size the PV array and battery system. The optimal sizing problem was solved for an optimization horizon of 1 year without accounting for battery capacity degradation as well as a 5-year optimization horizon taking into account yearly battery capacity degradation due to the calendar and cyclic aging. It was observed that the total system mass considering only the mass of PV array and battery systems are approximately in the range of 1.5×10^5 kg to 3.5×10^5 kg for the 1-year optimization horizon and 2×10^5 kg to 5.5×10^5 kg for the 5-year optimization horizon with a tower height of 10 m depending on different site's solar illumination profiles. For the same sites, if the tower height is increased to 50 m and further to 100 m, the total system mass varies approximately from 1×10^5 kg to 2.25×10^5 kg and from 1.5×10^5 kg to 3.25×10^5 kg for the 1-year and 5-year optimization horizons, respectively. Although increasing the tower height increases the total system mass due to the extra mass of the tower, the reduction of the battery mass is in the order of 10^5 kg. Moreover, tall towers can be used for other purposes such as lighting, long-distance communication, and power transmission using microwaves and lasers. To increase the reliability of the islanded space MG, this study also proposed designing the power system in the form of an MMG system. It was observed that the MMG system has approximately the same mass as a single islanded MG considering only the mass of required batteries and PV arrays for each MG. Evaluating the extra mass required for other equipment such as cables, power converters, protection systems, etc. is the subject of future studies by the authors. Finally, a criterion based on the total power demand served at a site and the corresponding total system mass was defined to identify the sites that serve the highest power demand with the least total system mass. Comparing the performance of different optimization algorithms for the sizing problem of space MGs is considered as a future work by the authors. In addition, studying the effects of uncertainties such as malfunctioning of equipment, communication system failure, or hitting system's infrastructures by meteors on the sizing of the PV-battery based MG is among the future research directions that are considered by the authors.

REFERENCES

[1] National Aeronautics and Space Administration (NASA). (2022). *NASA Artemis*. Accessed: Mar. 3, 2022. [Online]. Available: https://www.nasa.gov/specials/artemis/

[2] JAXA. (2022). *The JAXA Space Exploration Innovation Hub Center co-Produces Results on Remote and Automatic Control to Build Lunar Base*. Accessed: Mar. 3, 2022. [Online]. Available: https://global.jaxa.jp/press/2019/03/20190328a.html

[3] B. Westcott and J. Ogura. (2022). *Japan Wants to Put a Man on the Moon, Accelerating Asian Space Race*. Accessed: Mar. 3, 2022. [Online]. Available: https://edition.cnn.com/2017/06/29/asia/japan-moon-landing-jaxa/index.html

[4] N. Connor. (2022). *China Prepares for Manned Moon Landing*. Accessed: Mar. 3, 2022. [Online]. Available: https://www.telegraph.co.uk/news/2017/06/07/china-prepares-moon-landing/

[5] European Space Agency (ESA). (2022). *Imagining a Moon Base*. Accessed: Mar. 3, 2022. [Online]. Available: https://www.esa.int/Science_Exploration/Human_and_Robotic_Exploration/Imaginin g_a_Moon_base

[6] D. Etherington. (2022). *Spacex Wants to Land Starship on the Moon Before 2022, Then do Cargo Runs for 2024 Human Landing*. Accessed: Mar. 3, 2022. [Online]. Available: https://techcrunch.com/2019/10/25/spacex-wants-to-land-starship-on-the-moon-before-2022-then-do-cargo-runs-for-2024-human-landing/

[7] T. Mogg. (2022). *Prime Delivery, Straight From the Moon? Bezos Dreams of Heavy Industry in Space*. Accessed: Mar. 3, 2022. [Online]. Available: https://www.digitaltrends.com/cool-tech/jeff-bezos-reaffirms-plan-for-moon-colony/

[8] D. Saha, N. Bazmohammadi, J. M. Raya-Armenta, A. D. Bintoudi, A. Lashab, J. C. Vasquez, and J. M. Guerrero, "Space microgrids for future manned lunar bases: A review," *IEEE Open Access J. Power Energy*, vol. 8, pp. 570–583, 2021.

[9] A. J. Colozza. (2020). *Small Lunar Base Camp and In Situ Resource Utilization Oxygen Production Facility Power System Comparison*. [Online]. Available: https://ntrs.nasa.gov/citations/20200001622

[10] H. J. Fincannon. (2020). *Lunar Environment and Lunar Power Needs*. [Online]. Available: https://ntrs.nasa.gov/citations/20205002224

[11] J. F. Soeder, A. Mcnelis, R. Beach, N. McNelis, T. Dever, L. Trase, and R. May, "Overview of intelligent power controller development for human deep space exploration," in *Proc. 12th Int. Energy Convers. Eng. Conf.*, Jul. 2014, p. 3833.

[12] J. T. Csank, J. F. Soeder, M. A. Carbone, M. G. Granger, B. J. Tomko, M. J. Muscatello, and J. C. Follo, "A control framework for autonomous smart grids for space power applications," in *Proc. Int. Astron. Congr.*, 2019, pp. 1–6. [Online]. Available: https://ntrs.nasa.gov/citations/20190033175

[13] A. D. Bintoudi, C. Timplalexis, G. Mendes, J. M. Guerrero, and C. Demoulias, "Design of space microgrid for manned lunar base: Spinning-in terrestrial technologies," in *Proc. Eur. Space Power Conf. (ESPC)*, Sep. 2019, pp. 1–8.

[14] S. H. Choi, G. C. King, H.-J. Kim, and Y. Park. (2010). *Electrostatic Power Generation From Negatively Charged, Simulated Lunar Regolith*. [Online]. Available: https://ntrs.nasa.gov/citations/20100032922

[15] (2022). *Electrical Power—NASA Mars*. Accessed: Mar. 3, 2022. [Online]. Available: https://mars.nasa.gov/mars2020/spacecraft/rover/electrical-power/

[16] (2022). *Power | Rover—NASA's Mars Exploration Program*. Accessed: Mar. 3, 2022. [Online]. Available: https://mars.nasa.gov/msl/spacecraft/rover/power/
[17] E. B. Gietl, E. W. Gholdston, B. A. Manners, and R. A. Delventhal, "The electric power system of the international space station—A platform for power technology development," in *Proc. IEEE Aerosp. Conf.*, vol. 4, Mar. 2000, pp. 47–54.
[18] R. Pappa, C. Taylor, J. Warren, M. Chamberlain, S. Cook, S. Belbin, R. Lepsch, D. Tiffin, B. Doggett, M. Mikulas, I. Wong, D. Long, D. Steinkoening, A. Pensado, J. Blandino, and J. Haste. (Mar. 2021). *Relocatable 10 kw Solar Array for Lunar South Pole Missions—NASA Technical Reports Server (NTRS)*. Accessed: Dec. 12, 2022. [Online]. Available: https://ntrs.nasa.gov/citations/20210011743
[19] R. P. Mueller. (Jan. 2022). *Lunar Base Construction Overview—NASA Technical Reports Server (NTRS)*. Accessed: Dec. 12, 2022. [Online]. Available: https://ntrs.nasa.gov/citations/20220000418
[20] J. Fincannon, "Lunar polar illumination for power analysis," in *Proc. 6th Int. Energy Convers. Eng. Conf. (IECEC)*, Jul. 2008, p. 5631.
[21] J. Fincannon, "Characterization of lunar polar illumination from a power system perspective," in *Proc. 46th AIAA Aerosp. Sci. Meeting Exhib.*, Jan. 2008, p. 447.
[22] J. Freeh, "Analysis of stationary, photovoltaic-based surface power system designs at the lunar south pole," in *Proc. AIAA SPACE Conf. Expo.*, Sep. 2008, p. 7810.
[23] E. Mazarico, G. A. Neumann, D. E. Smith, M. T. Zuber, and M. H. Torrence, "Illumination conditions of the lunar polar regions using LOLA topography," *Icarus*, vol. 211, no. 2, pp. 1066–1081, Feb. 2011.
[24] P. Gläser, J. Oberst, G. Neumann, E. Mazarico, E. Speyerer, and M. Robinson, "Illumination conditions at the lunar poles: Implications for future exploration," *Planet. Space Sci.*, vol. 162, pp. 170–178, Jan. 2018.
[25] E. J. Speyerer and M. S. Robinson, "Persistently illuminated regions at the lunar poles: Ideal sites for future exploration," *Icarus*, vol. 222, no. 1, pp. 122–136, Jan. 2013.
[26] J. Fincannon, "Lunar south pole illumination: Review, reassessment, and power system implications," in *Proc. 5th Int. Energy Convers. Eng. Conf. Exhib. (IECEC)*, Jun. 2007, p. 4700.
[27] J. Oberst, A. Christou, R. Suggs, D. Moser, I. J. Daubar, A. S. McEwen, M. Burchell, T. Kawamura, H. Hiesinger, K. Wünnemann, R. Wagner, and M. S. Robinson, "The present-day flux of large meteoroids on the lunar surface—A synthesis of models and observational techniques," *Planet. Space Sci.*, vol. 74, no. 1, pp. 179–193, Dec. 2012.
[28] H. Benaroya, "Reliability and damage," in *Building Habitats on the Moon Engineering Approaches to Lunar Settlements*. Cham, Switzerland: Springer, 2018, pp. 249–285.
[29] W. P. Schonberg, F. Schäfer, and R. Putzar, "Some comments on the protection of lunar habitats against damage from meteoroid impacts," *J. Aerosp. Eng.*, vol. 23, no. 1, pp. 90–97, Jan. 2010.
[30] D. E. Smith, M. T. Zuber, G. A. Neumann, F. G. Lemoine, E. Mazarico, M. H. Torrence, J. F. McGarry, D. D. Rowlands, J. W. Head, T. H. Duxbury, O. Aharonson, P. G. Lucey, M. S. Robinson, O. S. Barnouin, J. F. Cavanaugh, X. Sun, P. Liiva, D.-D. Mao, J. C. Smith, and A. E. Bartels, "Initial observations from the lunar orbiter laser altimeter (LOLA)," *Geophys. Res. Lett.*, vol. 37, no. 18, pp. 1–10, Sep. 2010.
[31] M. K. Barker, E. Mazarico, G. A. Neumann, D. E. Smith, M. T. Zuber, and J. W. Head, "Improved LOLA elevation maps for south pole landing sites: Error estimates and their impact on illumination conditions," *Planet. Space Sci.*, vol. 203, Sep. 2021, Art. no. 105119.
[32] X. F. Zhao, A. Aierken, M. Heini, M. Tan, Y. Y. Wu, S. L. Lu, R. T. Hao, J. H. Mo, Y. Zhuang, X. B. Shen, Y. Xu, Q. Q. Lei, and Q. Guo, "Degradation characteristics of electron and proton irradiated InGaAsP/InGaAs dual junction solar cell," *Sol. Energy Mater. Sol. Cells*, vol. 206, Mar. 2020, Art. no. 110339.
[33] E. F. Lisbona, "LLF-2—Calibration, testing and monitoring of space solar cells," in *Solar Cells*, T. Markvart and L. Castañer, Eds. Oxford, U.K.: Elsevier, 2005, pp. 475–503.
[34] E. Sefton-Nash, M. Siegler, and D. Paige, "Thermal extremes in permanently shadowed regions at the lunar south pole," in *Proc. 44th Lunar Planet. Sci. Conf.*, 2013, p. 2617.
[35] D. M. Hurley, M. Sarantos, C. Grava, J.-P. Williams, K. D. Retherford, M. Siegler, B. Greenhagen, and D. Paige, "An analytic function of lunar surface temperature for exospheric modeling," *Icarus*, vol. 255, pp. 159–163, Jul. 2015.
[36] A. Pérez, M. Benavides, H. Rozas, S. Seria, and M. Orchard, "Guidelines for the characterization of the internal impedance of lithium-ion batteries in PHM algorithms," *Int. J. Prognostics Health Manage.*, vol. 9, no. 3, pp. 1–10, Nov. 2020.
[37] (2022). *7.0 Thermal Control | NASA*. Accessed: Mar. 3, 2022. [Online]. Available: https://www.nasa.gov/smallsat-institute/sst-soa-2020/thermal-control
[38] T. W. Kerslake and M. S. El-Genk, "Lunar surface-to-surface power transfer," in *Proc. AIP Conf.*, 2008, pp. 466–473.
[39] M. Kaczmarzyk, A. Starakiewicz, and A. Waśniowski, "Internal heat gains in a lunar base—A contemporary case study," *Energies*, vol. 13, no. 12, p. 3213, Jun. 2020.
[40] C. Ciurans, N. Bazmohammadi, J. C. Vasquez, G. Dussap, J. M. Guerrero, and F. Godia, "Hierarchical control of space closed ecosystems: Expanding microgrid concepts to bioastronautics," *IEEE Ind. Electron. Mag.*, vol. 15, no. 2, pp. 16–27, Jun. 2021.
[41] A. Colozza, R. Heller, W. Wong, and A. Hepp, "Solar energy systems for lunar oxygen generation," in *Proc. 48th AIAA Aerosp. Sci. Meeting Including New Horizons Forum Aerosp. Expo.*, Jan. 2010, p. 1166.
[42] T. Nakamura and B. Smith, "Solar power system for lunar ISRU applications," in *Proc. 48th AIAA Aerosp. Sci. Meeting Including New Horizons Forum Aerosp. Expo.*, Jan. 2010, p. 1162.
[43] P. E. C. Gordon, A. J. Colozza, A. F. Hepp, R. S. Heller, and R. Gustafson, "Thermal energy for lunar in situ resource utilization: Technical challenges and technology opportunities," in *Proc. 49th AIAA Aerosp. Sci. Meeting Including New Horizons Forum Aerosp. Expo.* Cleveland, OH, USA: NASA, 2011, p. 704.
[44] L. Mason and M. Rucker, "Common power and energy storage solutions to support lunar and Mars surface exploration missions," in *Proc. Int. Astron. Congr.*, 2019, pp. 1–7. [Online]. Available: https://ntrs.nasa.gov/citations/20190032521
[45] J. Blosiu, R. Bugga, E. Brandon, M. Smart, J. Elliott, J. Castillo, T. Yi, L. Lee, M. Piszczor, T. Miller, C. Reid, C. Taylor, S. Liu, U. S. Army, E. Plichta, C. Iannello, P. M. Beauchamp, and J. A. Cutts. (Dec. 2017). *Energy Storage Technologies for Future Planetary Science Missions Work Performed Under the Planetary Science Program Support Task*. [Online]. Available: https://solarsystem.nasa.gov/resources/549/energy-storage-technologies-for-future-planetary-science-missions/
[46] Z. Khan, "Power system concepts for the lunar outpost: A review of the power generation, energy storage, power management and distribution (PMAD) system requirements and potential technologies for development of the lunar outpost," in *Proc. AIP Conf.*, 2006, pp. 1083–1092.
[47] S. X. Chen, H. B. Gooi, and M. Q. Wang, "Sizing of energy storage for microgrids," *IEEE Trans. Smart Grid*, vol. 3, no. 1, pp. 142–151, Mar. 2012.
[48] B. Xu, A. Oudalov, A. Ulbig, G. Andersson, and D. S. Kirschen, "Modeling of lithium-ion battery degradation for cell life assessment," *IEEE Trans. Smart Grid*, vol. 9, no. 2, pp. 1131–1140, Mar. 2018.
[49] S. Ruppert, A. Ross, J. Vlassak, and M. Elvis, "Tall towers on the moon," 2021, *arXiv:2103.00612*.
[50] NASA. (2022). *Industry Mature Vertical Solar Arrays for Lunar Surface | NASA*. Accessed: Feb. 23, 2022. [Online]. Available: https://www.nasa.gov/feature/nasa-industry-to-mature-vertical-solar-array-technologies-for-lunar-surface

DIPTISH SAHA (Student Member, IEEE) received the B.Tech. degree in electronics and electrical engineering and the M.Tech. degree in electrical engineering–power electronics and drives from the Kalinga Institute of Industrial Technology (KIIT) University, Odisha, India, in 2013 and 2015, respectively. He is currently pursuing the Ph.D. degree with the Center for Research on Microgrids (CROM), Department of Energy Technology, Aalborg University, Denmark. His research interests include energy management of space microgrids and multi-microgrid systems.

NAJMEH BAZMOHAMMADI (Member, IEEE) received the B.S. degree in electrical engineering and the M.S. degree in electrical engineering–control from the Ferdowsi University of Mashhad, Iran, in 2009 and 2012, respectively, and the Ph.D. degree in electrical engineering–control from the K. N. Toosi University of Technology, Tehran, Iran, in 2019. She is currently a Postdoctoral Fellow with the Center for Research on Microgrids (CROM), Department of Energy Technology, Aalborg University, Denmark. Her current research interests include energy management of hybrid and renewable-based microgrids and multi-microgrids systems.

JOSÉ MAURILIO RAYA-ARMENTA received the B.Sc. degree in electrical engineering (power systems) and the M.Sc. degree in electrical engineering (signal processing) from the University of Guanajuato, México, in 2012 and 2015, respectively, and the Ph.D. degree in electrical engineering (space PV systems) from the Center for Research on Microgrids (CROM), AAU Energy, Aalborg University, Denmark, in 2022. He is currently an Electrical Design Engineer with SGRE (Research and Development), Brande, Denmark. His research interests include design, physical modeling, and simulation of PV+converter+battery systems, control schemes, and physics of radiation-induced degradation of III-V/Si-based PV-cells.

ANGELINA D. BINTOUDI (Member, IEEE) received the Diploma degree in electrical and computer engineering from the Faculty of Technology, Aristotle University of Thessaloniki, Greece, in July 2013. She is currently pursuing the Ph.D. degree with the Electrical Machines and Power Electronics Laboratory, Department of Electrical Energy, School of Electrical and Computer Engineering, Aristotle University of Thessaloniki. Her dissertation topic is the design and control of space microgrids.

From July 2014 to June 2015, she worked as a Designer of power supplies and power processing units for aerospace applications, under projects of the European Space Agency in an Italian private company. She has been employed with the Informatics and Technology Institute (I.T.I.), Centre for Research and Technology-Hellas (CE.R.T.H.), since June 2017. She has participated as a Senior Engineer in more than eight H2020 projects, three of which she has technically managed. Her research interests include space microgrids, stand-alone power systems, ac and dc microgrids, optimization, and multi-agent systems.

Ms. Bintoudi has been serving as a reviewer for several IEEE, IET, and Elsevier journals.

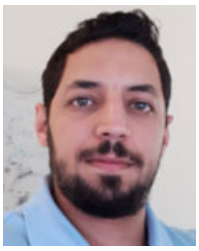

ABDEREZAK LASHAB (Senior Member, IEEE) received the Baccalaureate degree (Hons.) from the High School, Cheikh Ibrahim Bayoud, Constantine, Algeria, in 2007, the bachelor's and master's degrees in electrical engineering from the Université des Frères Mentouri Constantine 1, Constantine, in 2010 and 2012, respectively, and the Ph.D. degree in developing and investigating new converter topologies and control methods of photovoltaic systems with and without storage from the Department of Energy Technology, Aalborg University, Denmark, in 2019.

From 2012 to 2013, he worked as an Engineer at High Tech Systems (HTS). From 2013 to 2016, he was a Research Assistant at the Université des Frères Mentouri Constantine 1, where he helped in teaching several electrical engineering courses for undergraduate students. From April 2019 to July 2019, he was a Visiting Researcher at the Chair of Power Electronics, Kiel University, Germany. He is currently a Postdoctoral Researcher with Aalborg University. His current research interests include power electronics topologies, modeling, and control for photovoltaic systems with and without storage.

Dr. Lashab serves as a Reviewer for the IEEE TRANSACTIONS ON INDUSTRIAL ELECTRONICS, IEEE TRANSACTIONS ON POWER ELECTRONICS, IEEE TRANSACTIONS ON INDUSTRIAL INFORMATICS, IEEE TRANSACTIONS ON SUSTAINABLE ENERGY, *IET Power Electronics*, *IET Electronics Letters*, and several IEEE conferences.

JUAN C. VASQUEZ (Senior Member, IEEE) received the B.Sc. and Ph.D. degrees from UAM, Colombia, and the Ph.D. degree from UPC, Spain. In 2019, he was a Professor of energy internet and microgrids. He is currently the Co-Director of the Villum Center for Research on Microgrids. He has published more than 450 journal articles cited more than 30000 times. His research interests include operation, control, energy management applied to ac/dc microgrids, the integration of IoT, energy internet, digital twin, and blockchain solutions. He has been awarded as a Highly Cited Researcher, since 2017. He was a recipient of the Young Investigator Award, in 2019.

JOSEP M. GUERRERO (Fellow, IEEE) received the B.S. degree in telecommunications engineering, the M.S. degree in electronics engineering, and the Ph.D. degree from the Technical University of Catalonia, Barcelona, in 1997, 2000, and 2003, respectively. In 2019, he was a Villum Investigator at the Villum Fonden, which supports the Center for Research on Microgrids (CROM), Aalborg University, Denmark. Since 2011, he has been a Full Professor with the Department of Energy Technology, Aalborg University. His research interests include different microgrid aspects, including applications as remote communities, energy prosumers, and maritime and space microgrids.